Accepted Manuscript

Lenvatinib-zinc phthalocyanine conjugates as potential agents for enhancing synergistic therapy of multidrug-resistant cancer by glutathione depletion

Gaofei Wei, Liangfeng Huang, Yali Jiang, Yifeng Shen, Zeqian Huang, Yanjuan Huang, Xiaoqi Sun, Chunshun Zhao

PII: S0223-5234(19)30189-8

DOI: https://doi.org/10.1016/j.ejmech.2019.02.065

Reference: EJMECH 11157

To appear in: *European Journal of Medicinal Chemistry*

Received Date: 30 January 2019

Revised Date: 23 February 2019

Accepted Date: 23 February 2019

Please cite this article as: G. Wei, L. Huang, Y. Jiang, Y. Shen, Z. Huang, Y. Huang, X. Sun, C. Zhao, Lenvatinib-zinc phthalocyanine conjugates as potential agents for enhancing synergistic therapy of multidrug-resistant cancer by glutathione depletion, *European Journal of Medicinal Chemistry* (2019), doi: https://doi.org/10.1016/j.ejmech.2019.02.065.

Lenvatinib-Zinc Phthalocyanine Conjugates as Potential Agents for Enhancing Synergistic Therapy of Multidrug-Resistant Cancer by Glutathione Depletion

Gaofei Wei[‡]*, *Liangfeng Huang*[‡], *Yali Jiang*[‡], *Yifeng Shen, Zeqian Huang, Yanjuan Huang, Xiaoqi Sun, Chunshun Zhao**

School of Pharmaceutical Sciences, Sun Yat-sen University, Guangzhou 510006, China

Corresponding Author

* Chunshun Zhao E-mail: zhaocs@mail.sysu.edu.cn

* Gaofei Wei E-mail: weigaof@mail.sysu.edu.cn

Author Contributions

‡ These authors contributed equally.

Highlights

1. A photosensitive multifunctional conjugate ZnPc-C_8-Len was synthesized to realize photodynamic therapy to reverse multidrug resistance and enhanced antitumor therapy.
2. Upon the irradiation, ZnPc-C_8-Len could generate ROS to deplete intracellular GSH.
3. The decreased GSH would enhance apoptotic cell death by Bcl-2/caspase 3 pathway and reduce expression of P-gp to reverse lenvatinib resistance.
4. ZnPc-C_8-Len displayed significantly enhanced tumor accumulation and excellent *in vivo* antitumor activity.

Keywords

photodynamic therapy; targeted therapy; multidrug resistance; glutathione depletion; reactive oxygen species

ABSTRACT

The therapeutic efficacy of targeted therapy is dramatically hindered by multidrug resistance (MDR) because of elevated GSH levels. Thus, depletion of intracellular GSH level is highly desirable for targeted-therapeutic agents to reverse tumor drug resistance. In this study, a photosensitive multifunctional conjugate ZnPc-C_8-Len, in which lenvatinib (a VEGFR inhibitor) is linked to a photosensitizer ZnPc through an alkyl chains, was synthesized to realize photodynamic therapy to reverse multidrug resistance and enhanced antitumor therapy. Upon the irradiation, ZnPc-C_8-Len could generate ROS to deplete intracellular GSH. The decreased GSH would enhance apoptotic cell death by Bcl-2/caspase 3 pathway and reduce expression of P-gp to reverse lenvatinib resistance. Moreover, through PEG_{2000}-PLA_{2000} encapsulation, ZnPc-C_8-Len NPs displayed significantly enhanced tumor accumulation and excellent *in vivo* antitumor activity. And the fluorescence characteristics of ZnPc-C_8-Len could monitor the changes of nanoparticles *in vivo* in real time to guide when and where to conduct the subsequent therapy. As a result, conjugate ZnPc-C_8-Len had an outstanding capability to enhance synergistic therapy of multidrug-resistant cancer by glutathione depletion. And the approach reported here provide a promising strategy in development of conjugate integrated targeted therapy with photodynamic therapy to reverse targeted drug multidrug resistance and enhance synergistic therapy.

1. Introduction

Over the last few years, there is increasing evidence to demonstrate the prominent role of tyrosine kinases (TKs) in tumor initiation and progression.[1] Targeted therapies against the TKs (known as tyrosine kinase inhibitors or TKIs) have revolutionized the practice of oncology and a variety of TKIs have been developed, evaluated in clinical trials, and approved for cancer.[2] However, despite significant responses to TKIs, the majority of patients will develop multidrug resistant (MDR) to treatment within two years.[3] Therefore, effectively solving the problem of MDR becomes one of the biggest challenges in clinical applications.

MDR has been known to be associated with multiple factors, such as the alterations of drug target, the repair of DNA damage and blockade of drug-induced apoptosis, among which, high levels of glutathione (GSH) is correlated with a lot.[4-7] As a well-known intracellular antioxidant, GSH is widely expressed in normal tissues and cells as an important antioxidant that significantly attenuates oxidative stress level caused by toxic xenobiotics and reactive oxygen species (ROS).[8] Conceivably, increased GSH levels are a universal phenomenon in various types of cancer cells and solid tumors, and this tends to make these cells and tissues more resistant.[9, 10] The main reason for drug resistance is that GSH can conjugate therapeutic agents to facilitate their efflux by P-glycoprotein (P-gp), which is the one of most important proteins in MDR, and overexpressed in many tumors.[11, 12] GSH also is able to influence the apoptotic process by affecting Bcl-2 family anti-apoptotic proteins and caspase activity. Thus, depletion of intracellular GSH level is highly desirable for therapeutic agents to reverse tumor drug resistance.

Recently, photodynamic therapy (PDT) has been developed to reverse tumor resistance.[13-17] PDT is a noninvasive medical technology that employs ROS generated from photosensitizers

(PS) by light activation, triggering an apoptotic or necrotic response.[18] Excessive ROS can react rapidly with biological substrates GSH to disrupt the redox balance in cancer cells.[19, 20] PDT has also been demonstrated to cause the photo-destruction of P-gp by superabundant ROS. The reduction of P-gp expression facilitates the cytosolic retention delivery of therapeutic agents, resulting in a synergistic effect.[14, 16, 21-23]

Accordingly, an ideal scenario that integrates targeted therapy with photodynamic therapy can substantially overcome the MDR to enhanced antitumor therapy. Lenvatinib (Len) is first approved in 2015 as a vascular endothelial growth factor receptor (VEGFR) inhibitor, which is the majority of approved TKIs.[24] Unfortunately, Len remains severely multidrug resistant that is a substrate for the MDR transport protein P-glycoprotein (P-gp) (Eisai data on file).[25] For overcoming the drug resistance, PDT was recommended. Zinc phthalocyanine has strong tissue penetration and ROS production capacity under red-light.[26] In the present study, the preparation and anti-tumor activities of a conjugate (ZnPc-C_n-Len), in which Len is linked to a tetra (4-carboxyphenoxy)-zinc phthalocyanine (ZnPc) core through an alkyl chains with different lengths was reported. As illustrated in Scheme 1, upon the irradiation of red light, the conjugate ZnPc-C_n-Len generate ROS, which depletes intracellular GSH, thus resulting in down-regulation of P-gp and enhanced apoptotic cell death to reverse Len resistance. Also, the fluorescence bioimaging properties of conjugate can provide us with real-time information about when and where to apply the light illumination. The synergistic effect of Len and ZnPc can enhance anti-tumor effects *in vitro* and *in vivo*. Herein, this report demonstrates that the rationally designed conjugate ZnPc-C_n-Len has 'all in one' mode of anticancer actions to reverse multidrug resistance with synergistic effects in the proof of concept studies in *vitro* as well as in *vivo*.

2. Results and Discussion

2.1 Synthesis of ZnPc-C_n-Len.

The ZnPc and Len were covalently linked by a flexible carbon chain, which can improve the biocompatibility of the conjugate while maintaining the maximum targeting capacity of Len. The synthesis of ZnPc was prepared according to our reported procedures.[27] The synthesis methods of the conjugates ZnPc-C_0-Len, ZnPc-C_8-Len and ZnPc-C_{12}-Len were demonstrated in Scheme 2. The detailed structure of ZnPc-C_0-Len, ZnPc-C_8-Len and ZnPc-C_{12}-Len were confirmed by FTIR spectrum (Figure 1A) and Matrix-Assisted Laser Desorption/Ionization Time of Flight Mass Spectrometry (MALDA-TOF-MS) (Figure S16–S18, Supporting Information). As showed in Figure 1A, the vibration bands centered at 2920 cm^{-1} (-CH) and 1369 cm^{-1} (-CH) are corresponding to the alkane belong to ZnPc-C_8-Len and ZnPc-C_{12}-Len. Moreover, the stretching vibrations of -NH-, -C=O- and -C-O-C- are around 3338, 3177, 1655 and 1229 cm^{-1} respectively in the spectra of ZnPc-C_n-Len, which were the representative peaks of Len segment. These results of the above FTIR data confirmed that Len has been successfully covalently conjugated with zinc phthalocyanine. And ZnPc-C_n-Len demonstrated the similar UV/vis absorbance to ZnPc (Figure 1B). Moreover, the maximum excitation wavelength and emission wavelength of ZnPc-C_8-Len were at 681 nm and 687 nm respectively (Figure 1C). The fluorescence spectroscopy of ZnPc, ZnPc-C_0-Len and ZnPc-C_{12}-Len were showed at Figure S1-S3. The fluorescence spectroscopy of ZnPc-C_n-Len was similar to ZnPc and suggested that ZnPc-C_n-Len may have a parallel photosensitivity of ZnPc.

2.2 *In Vitro* ROS Generation

The ROS production capacity of three conjugates ZnPc-C_n-Len upon light irradiation were first investigated. The generation of ROS was indicated by DBPF as a ROS sensitive probe. DPBF could rapidly capture and react with ROS, then reduce its absorbance at 416 nm. As shown in

Figure 1D, upon the irradiation, DPBF was degraded rapidly in the present of ZnPc or ZnPc-C_n-Len, whereas the group of purely DBPF declared no significant degradation upon the same irradiation, which confirmed the capacity of ROS generation of ZnPc-C_n-Len with light irradiation. Then the photobleaching of ZnPc-C_n-Len were evaluated in Figure S4, which confirmed that ZnPc-C_n-Len possessed a great photostability during the ROS generation.

2.3 Anticancer efficiency of ZnPc-C_n-Len.

First, to evaluate the anticancer efficiency of three derivatives, the MTT assay was used to detect cell viability compared with free Len, free ZnPc and ZnPc/Len (equimolar mixture) and ZnPc-C_n-Len against MCF7 cells (20 μM), MCF7/ADR cells (100 μM) and 4T1 cells (20 μM) respectively. As shown in Figure 2, in the absence of irradiation, free Len and ZnPc/Len (equimolar mixture) exhibited cell cytotoxicity rates of 30.16% and 28.71% against MCF7 cells. But conjugates ZnPc-C_0-Len, ZnPc-C_8-Len and ZnPc-C_{12}-Len showed lower cell cytotoxicity rates of 9.52%, 27.23% and 19.27%, respectively. From the above dark cytotoxicity data, it was verified that the modification of a bulky group on the amino group of Len reduced slight activity of Len. Among the dark cytotoxicity of three conjugates, ZnPc-C_8-Len conjugate showed the least decrease compared to the prototype drug Len, which might be possible that the alkyl chains of eight carbons have the least effect on the binding of Len and its target protein. The above same phenomenon was also observed in drug-resistant MCF7/ADR cells and 4T1 cells. However, under a relatively low light dose (660-670 nm, 50 mW cm^{-2}, 10 min), all three conjugates show significantly higher cytotoxicity than Len in all of three cancer cells, among which ZnPc-C_8-Len conjugate showed the strongest cytotoxicity and MDR reversal efficacy with 74.71% for MCF7 cells, 74.55% for MCF7/ADR cells and 49.71% for 4T1 cells respectively. More interestingly, the cytotoxicity of Len in drug-resistant MCF7/ADR cells was almost

negligible (approximately 18%), but the activity of Len modified photosensitizer (ZnPc-C_8-Len) was significantly increased with irradiation, which suggested that the conjugated form can increase the activity of Len in drug-resistant cells. Thus, from above the cell viability, it was reasonable to infer that the covalent combination of photosensitizer and Len can effectively improve cytotoxic activity even in drug-resistant cells.

2.4 Correlation between GSH and Len-resistance.

With the above desirable observation of significant cytotoxicity and MDR reversal efficacy of ZnPc-C_n-Len and the previous reports about GSH participates in the development of various multidrug-resistance cells,[28, 29] it is suspicious that whether Len is cross-resistant to MCF7/ADR cells and whether GSH was involved in Len-cross-resistant. To elucidate the first concern, both MCF7 and MCF7/ADR cells were investigated for their sensitivity towards Len. MCF7 and MCF7/ADR cells were seeded in 96-well plates and exposed to different concentrations of Len for 24 h. Cell viability tested by MTT assay indicated that MCF7/ADR cells were less sensitive towards Len (Figure 3A and 3B). Noteworthy, high dose (42.9 μM) of Len that sufficed to reduce MCF7 viability to 50% only reduced MCF7/ADR cells viability to 95%. These results agreed well with the surmise that Len was indeed resistant to MCF7/ADR cells.

Then whether GSH contributed to Len cross-resistance observed in MCF7/ADR was investigated. MCF7 and MCF7/ADR cells were pretreated with BSO (buthionine sulfoximine, a GSH synthetase inhibitor) or exogenous GSH, then tested for their sensitivity towards various concentrations of Len. Firstly, GSH and BSO itself were confirmed to have no toxicity on cell growth after 72 h exposure (Figure S5 and S6). Then cells were incubated with BSO (500 μM) or GSH (2.5 mM) for 24 h to disrupt GSH balance, followed by being exposed to Len to test the sensitivity. As shown in Figure 3, the results suggested that the combined application of BSO

could increase the cytotoxicity of Len. Compared with MCF7 cells (~2 -fold, from 73.1 μM to 42.9 μM), a significant decrease of the IC_{50} values was found in MCF7/ADR cells (~5 -fold, 291.5 μM to 58.8 μM). On the contrary, the concomitant application of exogenous GSH reduced the sensitivity of Len, with 1.4-fold improvement of the IC_{50} values in MCF7/ADR cells and 1.2-fold in MCF7. Combine the above results, it can be clearly obtained the correlation between GSH and Len-resistance in MCF7/ADR cells.

2.5 Monitoring GSH change

To shed light on the mechanism of Len-resistance, ZnPc-C_8-Len was chosen as a representative compound to investigate the subsequent studies because it had the strongest cytotoxicity and MDR reversal efficacy. First, the level of GSH in MCF7 and MCF7/ADR cells impacted by ZnPc-C_8-Len was investigated. Cells were treated with ZnPc-C_8-Len, BSO, Len and ZnPc for 24 h follow by exposing to irradiation for 10 min and then the level of GSH was quantitatively measured. As shown in Figure 4, Free Len could slightly increase GSH level in MCF7/ADR cells. This observation can be explained by the rationales that MDR cells can launch robust GSH biosynthetic system to produce GSH to detoxify therapeutic agents through phase II metabolism.[4, 30, 31] However, treatment of BSO, ZnPc or ZnPc-C_8-Len resulted in significant reduction of the GSH level. Compared with MCF7 cells, a more significant decrease of GSH levels by ZnPc-C_8-Len was found in MCF7/ADR cells. Through the above experiments, it can be reasonably concluded that conjugate ZnPc-C_8-Len could efficiently deplete GSH in MCF7 and MCF7/ADR cells.

2.6 Mechanism of MDR Reversal

Resistant cells increase the capacity of tolerating therapy drugs by high GSH levels mediated escaping apoptosis.[4] Nevertheless, ZnPc-C_8-Len was convincingly verified to effectively deplete

GSH in MCF7/ADR cells. Naturally, it can be conjectured that ZnPc-C_8-Len could alleviate apoptotic silence to reverse MDR. To test this hypothesis, the apoptosis induced by ZnPc-C_8-Len in MCF7 and MCF7/ADR cells was measured by Annexin V-FITC/PI double staining assay. After incubation with free Len, the apoptosis rate of the MCF7 cells was 44.1%, respectively, but only 16.3% in the MCF7/ADR cells (Figure 5A). This result was consistent with accepted knowledge that apoptosis can be silenced in drug-resistant cells. Compared with free drug formulation, it was discovered that ZnPc-C_8-Len promoted much higher level of apoptosis in both MCF7 and MCF7/ADR cells with 82.4% and 75.0%. Thus, the outstanding performance of apoptosis activation by ZnPc-C_8-Len in MCF7/ADR may lead to a better therapeutic outcome.

After obtaining the above results, the probable mechanism of apoptosis caused by ZnPc-C_8-Len was investigated. The previous studies have showed that drug resistance mediated from high GSH concentration is associated with overexpression of anti-apoptotic protein Bcl-2 which is known as an important gatekeeper to the apoptotic response.[32, 33] Next, western blot was used to analyze the level of Bcl-2 expression in both MCF7 and MCF7/ADR cells with ZnPc-C_8-Len. As shown in Figure 5B and 5D, after exposure of MCF7 or MCF7/ADR cells to ZnPc-C_8-Len with irradiation, the expression of Bcl-2 protein was significantly decrease compared to free Len.

Furthermore, Caspase 3, the downstream protein of Bcl-2 and the essential executioner caspase required for apoptosis signaling were also investigated. [34] It was obviously that ZnPc-C_8-Len upregulated the expression of apoptosis related cleaved-caspase 3 in MCF7/ADR cells (Figure 5B and 5E). All these results indicated that ZnPc-C_8-Len is more efficiently decrease the expression of Bcl-2, thus activating caspase 3 to promote MCF7/ADR cell apoptosis compared with the single free drug Len.

However, there may be another reason that ZnPc-C_8-Len could induce greater apoptosis in MCF7/ADR cells, which is probably due to the enhanced intracellular drug accumulation by reducing the efflux of the drug. As well-known, P-gp, an efflux pump transporter, was able to increase Len efflux and cause therapy failure.[35] Thus, the expression level and activity of P-gp will make a great contribution to the MDR effect. In order to confirm this hypothesis, the expression of P-gp after treating with ZnPc-C_8-Len in MCF7/ADR cells was investigated. As shown in Figure 5C and 5F, the expression of P-gp was downregulated significantly by ZnPc-C_8-Len upon the irradiation in the MCF7/ADR cells. In brief, it could be inferred that the mechanism of MDR reversal might lie on the induction of apoptosis through down-expression of Bcl-2 and up-expression of caspase 3 accompanied with the reduction of P-gp expression.

2.7 *In vitro* cytotoxicity evaluation

First, intracellular drug accumulation efficiency of ZnPc-C_8-Len in MCF7 and MCF7/ADR cells were evaluated by confocal laser scanning microscopy (CLSM). Cells were incubated with ZnPc-C_8-Len for 24 h to arrive a same absorbance (Figure S7) before the different treatment. Then cells were rinsed with PBS and incubated with fresh culture medium to investigate the drug retention. As shown in Figure 6A, MCF7 cells presented higher fluorescence intensity than MCF7/ADR cells under no light irradiation. This can be explained that MCF7/ADR increased efflux of ZnPc-C_8-Len assisted by overexpressed P-gp, resulting in limited drug accumulation in cells. In contrast, upon light irradiation, the intracellular fluorescence intensity became obviously stronger in MCF7/ ADR cells which may be due to the decrease of the expression of P-gp. Such improvement of intracellular drug retention of ZnPc-C_8-Len was also observed in MCF7/ADR cells with the treatment of verapamil, which is a P-gp inhibitor. Taken together, the findings confirmed that ZnPc-C_8-Len could indeed accumulate effectively inside MCF7/ADR cells.

Subsequently, its cytotoxicity against MCF7 cells, 4T1 cells and MCF7/ADR cells were tested (Figure 6B, 6C & 6D), and IC_{50} values were calculated and summarized in Table S1. The IC_{50} values of ZnPc-C_8-Len against 4T1 cells was 19.4 μM compared with 67.7 μM for Len, a 3.5-fold decrease, and a 4.5-fold decrease against MCF7 cells correspondingly. More importantly, ZnPc-C_8-Len showed a significantly improved cytotoxicity against MCF7 /ADR cells, with an IC_{50} values 47.32 μM while 329.2 μM for Len, a 6.9-fold decrease, indicating that ZnPc-C_8-Len could indeed reverse MDR in cancer cells.

To evaluate the synergistic effect between ZnPc and Len, the combination index (CI) of ZnPc-C_8-Len was calculated according to Equation (1).[36] And the CI index indicates antagonism (CI >1), additivity (CI = 1), or synergism (CI <1) between the drugs. ZnPc and Len conjugated in ZnPc-C_8-Len were synergistic against all three cell lines, with CI values of 0.82, 0.80 and 0.42 in the 4T1, MCF7, and MCF7/ADR cell lines, respectively. In the MCF7/ADR cells, the CI values was much lower than that in other cancer cells 4T1 and MCF7, indicating an excellent synergistic effect in the drug resistant strain. The synergy in MCF7 ADR suggested that ZnPc-C_8-Len might minimize drug resistance in cancer cells.

2.8 *In vivo* antitumor efficacy

The *in vivo* therapeutic effects and potent toxicity were eventually verified on the tumor bearing mice. Therapeutic nanoparticles (NPs) have been widely investigated to enhance cancer treatment. Because of the low solubility of ZnPc-C_8-Len, it was loaded into biodegradable PEG_{2000}-PLA_{2000} nanoparticles to improve solubility. In addition, ZnPc-C_8-Len nanoparticles can be accumulated in tumor tissues after tail vein injection due to enhanced permeability and retention (EPR) effects. At the same time, the fluorescence characteristics of ZnPc-C_8-Len can

be utilized to monitor the changes of nanoparticles *in vivo* in real time so as to guide when and where to conduct the subsequent therapy.

First, Len, ZnPc and ZnPc-C_8-Len can be formulated in PEG_{2000}-PLA_{2000} to form nanoparticles of a uniform diameter around 124, 167 and 151 nm for Len NPs, ZnPc NPs and ZnPc-C_8-Len NPs respectively (Figure S8 and S9). ZnPc-C_8-Len NPs still had the ability to produce ROS generation (Figure S10). The antitumor efficacy of ZnPc-C_8-Len NPs was also investigated in 4T1 cells (Figure S11).

Then *in vivo* imaging experiment was performed using the fluorescence properties of ZnPc-C_8-Len NPs. As shown in Figure 7A, for ZnPc-C_8-Len NPs, fluorescence was clearly observed at tumor site after 3 h post-injection. More importantly, 24 hours after the injection, clear fluorescence signals could still be observed at the tumor site. These results suggested that the tumor accumulation of ZnPc-C_8-Len NPs could be real-time monitored by the fluorescence changes. Moreover, according to the fluorescence intensity, the distribution of ZnPc-C_8-Len NPs in different tissues was compared. As shown in Figure 7B, after 24 h of injection, ZnPc-C_8-Len NPs accumulated mainly in tumor tissue, while the accumulation in other tissues was tolerable. Figure 7C represents the mean fluorescence intensity of ZnPc-C_8-Len in the tumor and other organs, and the result was consistent with that found in Figure 7B. In all, after the encapsulation of ZnPc-C_8-Len into PEG_{2000}-$PLGA_{2000}$, ZnPc-C_8-Len could efficiently accumulate in tumor tissue and stay in tumor for long time, which will favor the enhanced antitumor effect *in vivo*.

Thus, the antitumor efficacy of ZnPc-C_8-Len NPs in vivo was tested via intravenous injection. As shown in Figure 7D, without irradiation, the normal saline groups and ZnPc NPs groups had almost no effect on tumor growth. ZnPc-C_8-Len NPs could slightly inhibit tumor growth, and moderate therapeutic efficacy of Len NPs was observed in the mice administrated. This result

was consistent with the conclusion that the modification of a bulky group on the amino group of Len could reduce slight the anti-tumor activity of Len in the absence of light *in vitro* cell experiments. And light irradiation had little effect on the anti-tumor effect of Len NPs, but light had substantial effect on ZnPc NPs due to PDT. After light irradiation with 671 nm, the antitumor activity of ZnPc NPs was similar to that of Len NPs. However, ZnPc-C_8-Len NPs display the best therapeutic efficacy and almost completely depress the tumor progression after light irradiation. After PDT treatment, tumors were excised for photographing (Figure 7E) and weighing (Figure 7F). During the treatment, body weight of mice was record and no significantly changes were observed (Figure 7G).

To further evaluate the therapeutic effects, standard H&E staining analysis of tumor tissues and organs was performed. From H&E staining images (Figure 8A), some tumor cells were damaged in the Len NPs group and ZnPc-C_8-Len NPs group without light irradiation, which should be the contribution of Len. ZnPc NPs group with light irradiation also had some tumor cell damage, which should be the contribution of PDT of ZnPc. There was a large area of cell damage in ZnPc-C_8-Len NPs group with laser irradiation, which should be the synergistic effect of photodynamic and targeted therapy. Moreover, major organs (liver, spleen, kidney, heart and lung) were collected and sliced for H&E staining (Figure 8B). No obvious sign of organ damage or inflammatory lesion was observed. All these results suggested ZnPc-C_8-Len NPs would be a relatively safe agent with noninvasive in situ drug tracking and fluorescence imaging guided efficient antitumor therapy in vivo.

3. Conclusions

In summary, a photosensitive multifunctional conjugate ZnPc-C_8-Len was designed and synthesized to realize the photodynamic therapy to reverse multidrug resistance and enhanced

antitumor therapy. After the irradiation, the conjugate ZnPc-C_8-Len could generate ROS to deplete intracellular GSH. The decreased GSH would enhance apoptotic cell death by Bcl-2/caspase 3 pathway and reduce expression of P-gp to reverse lenvatinib resistance. *In vitro* ZnPc-C_8-Len could accumulate effectively inside MCF7/ADR cells and possessed an excellent synergistic effect. Moreover, through PEG_{2000}-PLA_{2000} encapsulation, ZnPc-C_8-Len nanoparticles can be accumulated in tumor tissues. At the same time, the fluorescence characteristics of ZnPc-C_8-Len can monitor the changes of nanoparticles *in vivo* in real time so as to guide when and where to conduct the subsequent therapy. With the guidance, ZnPc-C_8-Len NPs showed excellent *in vivo* antitumor activity. As a result, conjugate ZnPc-C_8-Len had an outstanding capability to enhance synergistic therapy of multidrug-resistant cancer by glutathione depletion. And the approach reported here provide a promising strategy in development of conjugate integrated targeted therapy with photodynamic therapy to reverse targeted drug multidrug resistance and enhance synergistic therapy.

4. Experimental Section

4.1 Materials

1-(2-chloro-4-hydroxyphenyl)-3-cyclopropylurea, Len, Methyl 4-chloro-7-Methoxyquinoline-6-carboxylate, 2',7'-Dichlorofluorescin diacetate (DCFH-DA), 1-ethyl-3-(3-dimethylaminopropyl)carbodiimide hydrochloride, 1,8-Diaminooctane, 1,12-Dodecanediamine, Fetal Bovine Serum (FBS), 3-(4,5-dimethyl-thiazol-2-yl)-2,5-diphenyl tetrazolium bromide (MTT), Dulbecco's modified Eagle's medium (DMEM), phosphate buffered saline (PBS), l- were purchased from Sigma-Aldrich (USA). Phenyl chloroformate, 3-Bromo-1-propanol, 4',6-Diamidino-2-phenylindole Dihydrochloride (DAPI), 9 10-anthracenediyl-bis(methylene) (ABDA), buthionine-sulfoximine (BSO), reduced glutathione (GSH) 1,3-Diphenylisobenzofuran

(DBPF), was obtained from Aladdin (China). PEG_{2000} -PLA_{2000} was purchased from Beijing HWRK Chem Co., LTD. GSH Assay Kit, P glycoprotein rabbit monoclonal antibody, β-actin mouse monoclonal antibody, HRP-labeled Goat Anti-Mouse IgG, HRP-labeled Goat Anti-Rabbit IgG was obtained from Beyotime Biotechnology Co., LTD. Other chemicals were of analytical grade and used without further purification. Preparative column chromatography was used with 200-300 mesh silica gel (Qingdao Haiyang Chemical, China). ^{1}H and ^{13}C NMR spectra were recorded on a Bruker ARX 600 MHz spectrometer. The purity of ZnPc-C_n-Len (≥ 95%) were determined by analytical HPLC. Analytical HPLC was performed at Hitachi L-2000 instrument equipped with a UV-DAD detector. The chromatographic separation was achieved on an C18 column, (150 mm × 3.9 mm, Nova-Pak-C18, Waters) at a flow rate of 1.0 mL/min in two mobile phases (THF-Distilled water=15:85).

4.2 Synthesis of ZnPc-C_n-Len

4-(3-chloro-4-(3-cyclopropylureido)phenoxy)-7-methoxyquinoline-6-carboxylate Methyl (S1)

10g (44.12 mmol) 1-(2-chloro-4-hydroxyphenyl)-3-cyclopropylurea and 8.88g (35.30 mmol) Methyl 4-chloro-7-Methoxyquinoline-6-carboxylate was dissolved in 150 mL DMF. Then 18.29 g (132.36 mmol) K_2CO_3 was added and the suspension was stirred at 75□ for 30 min. After that, the suspension was stirred at room temperature for 2 h and 500 mL distilled water was added. The precipitate was filtered and washed thoroughly with distilled water. After drying at vacuum, the precipitate was re-crystallize in methanol and dichloromethane (2:1, v/v) to get white crystal pure product with a yield of 89 %. ^{1}H NMR (400 MHz, DMSO-d_6) δ 8.70 (d, J = 5.3 Hz, 1H), 8.58 (s, 1H), 8.29 (d, J = 9.1 Hz, 1H), 7.99 (s, 1H), 7.57 – 7.47 (m, 2H), 7.26 (dd, J = 9.1, 2.8 Hz, 1H), 7.21 (d, J = 3.0 Hz, 1H), 6.54 (d, J = 5.3 Hz, 1H), 3.98 (s, 3H), 3.87 (s, 3H), 2.58 (dd, J

= 7.0, 3.5 Hz, 1H), 0.67 (dt, *J* = 6.8, 3.3 Hz, 2H), 0.43 (dt, *J* = 7.0, 3.5 Hz, 2H). ESI-MS (m/z): 442.1 $[M+H]^+$.

4-(3-chloro-4-(3-cyclopropylureido)phenoxy)-7-methoxyquinoline-6-carboxylic acid (S2) 10 g (22.63mmol) **S1** was dissolved in 100 mL methanol, 50 mL THF and 1 M NaOH solution. After stirred at 70□ for 2.5 h, the solution was cooled to room temperature and concentrated using rotary evaporator. Then, pH value of the mixture was buffered close to 4.5 using hydrochloric acid. The precipitate was filtered and washed thoroughly with distilled water. Finally, the white product **S2** was dried at vacuum and recrystallized in methanol and dichloromethane (2:1, v/v) with a yield of 92%. ^{1}H NMR (400 MHz, DMSO-d_6) δ 13.34 (s, 1H), 8.82 (d, *J* = 5.8 Hz, 1H), 8.61 (s, 1H), 8.32 (d, *J* = 9.1 Hz, 1H), 8.03 (s, 1H), 7.57 (d, *J* = 3.2 Hz, 2H), 7.31 (dd, *J* = 9.1, 2.8 Hz, 1H), 7.25 (d, *J* = 2.9 Hz, 1H), 6.73 (d, *J* = 5.8 Hz, 1H), 4.02 (s, 3H), 2.61 – 2.55 (m, 1H), 0.67 (dt, *J* = 6.7, 3.3 Hz, 2H), 0.48 – 0.38 (m, 2H). ESI-MS (m/z):426.1$[M-H]^-$.

N-(8-aminooctyl)-4-(3-chloro-4-(3-cyclopropylureido)phenoxy)-7-methoxy quinoline-6-carboxamide (S3). 500 mg (1.17 mmol) **S2**, 336.05 mg (1.75 mmol) EDCI and 337.18 mg (2.34 mmol) 1-Hydroxybenzotriazole (BtOH) was dissolved in DMF. The mixture was stirred at room temperature for 2 h. After that, the mixture was added to DMF solution of 1,8-Diaminooctane (337.18 mg, 2.34 mmol) and stirred at room temperature for 24 h. Then the mixture was added to distilled water and the precipitate was filtered and washed thoroughly with distilled water. The pure product **S3** was purified by column chromatography with a yield of 48%. ^{1}H NMR (400 MHz, DMSO-d_6) δ 8.67 (d, *J* = 5.2 Hz, 1H), 8.51 (s, 1H), 8.40 (t, *J* = 5.7 Hz, 1H), 8.27 (d, *J* = 9.1 Hz, 1H), 8.14 (s, 1H), 7.64 (s, 1H), 7.51 (s, 1H), 7.47 (d, *J* = 2.8 Hz, 1H), 7.23 (dd, *J* = 9.1, 2.8 Hz, 1H), 6.54 (d, *J* = 5.2 Hz, 1H), 4.02 (s, 3H), 3.30 (q, *J* = 6.7 Hz, 2H), 2.78 – 2.69 (m, 2H),

2.58 (dq, *J* = 7.0, 3.4 Hz, 1H), 1.54 (q, *J* = 7.2 Hz, 4H), 1.39 – 1.21 (m, 10H), 0.66 (dt, *J* = 6.8, 3.3 Hz, 2H), 0.49 – 0.39 (m, 2H). ESI-MS (m/z): 554.3 $[M+H]^+$.

N-(12-aminododecyl)-4-(3-chloro-4-(3-cyclopropylureido)phenoxy)-7-methoxy quinoline-6-carboxamide (S4). 500 mg (1.17 mmol) **S2**, 336.05 mg (1.75 mmol) EDCI and 337.18 mg (2.34 mmol) HoBt was dissolved in DMF. The mixture was stirred at room temperature for 2 h. After that, the mixture was added to DMF solution of 1,12-Dodecanediamine (468.31 mg, 2.34 mmol) and stirred at room temperature for 24 h. Then the mixture was added to distilled water and the precipitate was filtered and washed thoroughly with distilled water. The pure product **S4** was purified by column chromatography with a yield of 34%. ^{1}H NMR (400 MHz, DMSO-d_6) δ 8.66 (d, *J* = 5.3 Hz, 1H), 8.49 (s, 1H), 8.42 – 8.32 (m, 2H), 8.25 (d, *J* = 9.1 Hz, 1H), 7.79 (s, 1H), 7.51 (s, 1H), 7.45 (d, *J* = 2.8 Hz, 1H), 7.22 (dd, *J* = 9.1, 2.8 Hz, 1H), 6.53 (d, *J* = 5.2 Hz, 1H), 4.01 (s, 3H), 2.64 (t, *J* = 7.5 Hz, 2H), 2.60 – 2.54 (m, 1H), 1.72 (s, 4H), 1.51 (dt, *J* = 25.3, 6.7 Hz, 4H), 1.31 – 1.21 (m, 16H), 0.64 (dt, *J* = 6.8, 3.3 Hz, 2H), 0.43 (p, *J* = 4.6 Hz, 2H). ESI-MS (m/z): 610.3 $[M+H]^+$.

ZnPc-C$_0$-Len. 500 mg (0.45 mmol) ZnPc, 228.26 mg (0.54 mmol) Len, 128.14 mg (0.67 mmol) EDCI, 120.42 mg (0.89 mmol) HoBt and 90 μL N, N-Diisopropylethylamine was dissolved in DMF. The mixture was stirred at room temperature for 24 h and evaporated to yield a blue oil when reaction completed. Finally, the pure product was purified by column chromatography (CH_2Cl_2/CH_3OH/TEA 15:1:0.1) as a dark green solid with a yield of 15%. MALDI-TOF MS (m/z):1529.751 (Calcd for $[M+H]^+$: 1529.250). Chemical purity assessed by HPLC: 96.53%.

ZnPc-C$_8$-Len. 500 mg (0.45 mmol) ZnPc, 296.26 mg (0.54 mmol) **S3**, 128.14 mg (0.67 mmol) EDCI, 120.42 mg (0.89 mmol) HoBt and 90 μL N, N-Diisopropylethylamine was dissolved in DMF. The mixture was stirred at room temperature for 24 h and evaporated to yield a blue oil

when reaction completed. Finally, the pure product was purified by column chromatography (CH_2Cl_2/CH_3OH/TEA 15:1:0.1) as a dark green solid with a yield of 26%. MALDI-TOF MS (m/z):1656.602 (Calcd for $[M+H]^+$: 1656.386), 1678.611 (Calcd for $[M+Na]^+$: 1678.368). Chemical purity assessed by HPLC: 97.47%.

ZnPc-C_{12}-Len. 500 mg (0.45 mmol) ZnPc, 326.31 mg (0.54 mmol) S4, 128.14 mg (0.67 mmol) EDCI, 120.42 mg (0.89 mmol) HoBt and 90 μL N, N-Diisopropylethylamine was dissolved in DMF. The mixture was stirred at room temperature for 24 h and evaporated to yield a blue oil when reaction completed. Finally, the pure product was purified by column chromatography (CH_2Cl_2/CH_3OH/TEA 15:1:0.1) as a dark green solid with a yield of 19%. MALDI-TOF MS (m/z):1712.584 (Calcd for $[M+H]^+$: 1712.449), 1734.593 (Calcd for $[M+Na]^+$: 1734.431). Chemical purity assessed by HPLC: 96.02%.

4.3 Characterization of ZnPc-Len

UV−vis Spectroscopy. Len, ZnPc, ZnPc-C_0-Len, ZnPc-C_8-Len, ZnPc-C_{12}-Len were dissolved in DMSO at the same concentration of 5 μM. Then their UV-visible absorption spectra were recorded using an UV-vis spectrophotometer (TECHCOMP, UV2600 spectrophotometer).

Fluorescence Spectroscopy. ZnPc, ZnPc-C_0-Len, ZnPc-C_8-Len, ZnPc-C_{12}-Len were dissolved in DMSO at the same concentration. Then their fluorescence spectra were recorded using a spectrofluorophotometer (Fluoromax-4, Horiba, Japan). The fluorescence excitation spectra and emission spectra were obtained through monitoring emission wavelength at 780 nm and exciting at 560 nm, respectively.

Detection of ROS. Blank DMSO (control), ZnPc, ZnPc-C_0-Len, ZnPc-C_8-Len and ZnPc-C_{12}-Len were mixed with DBPF solution (60 μM) at a final concentration at 1 μM. After that, the mixture was exposed to laser irradiation (671 nm, 20 mW cm^{-2}) and the absorbance of the

mixture at 416 nm was recorded. The generation capacity of ROS of ZnPc, ZnPc-C_8-Len nanoparticles in aqueous solution was acquired using the similar method and ABDA was used as water soluble indicator. In brief, blank DMSO (control), ZnPc or ZnPc-C_8-Len nanoparticles were mixed with ABDA water solution (100 μM) at a final concentration of 5 μM (ZnPc equivalent dose). After that, the mixture was exposed to laser irradiation (671nm, 100 mW cm^{-2}) and the absorbance of mixture at 401 nm was recoreded. The DBPF and ABDA degradation rate was calculated as $(A_0-A_t)/A_0 \times 100\%$ (A_0: the absorbance of the mixture solution before irradiation, A_t: the absorbance after irradiation;)

Photostability. The photostability of ZnPc, ZnPc-C_0-Len, ZnPc-C_8-Len and ZnPc-C_{12}-Len during PDT was measured by their degradation reflected by the decrease of their absorbance. Photosensitizers were dissolved in DMSO at same concentration and exposed to laser irradiation (671 nm,100 mW cm^{-2}). And the photobleaching capacity was calculated as A_t/A_0. (A_0: the absorbance of mixture before irradiation, A_t: the absorbance after irradiation;)

4.4 Cellular assay

Cell culture. 4T1 murine breast carcinoma cells, MCF7 and MCF7/ADR (adriamycin drug-resistant) human breast carcinoma cells were obtained from Laboratory Animal Center of Sun Yat-sen University (Guangzhou, China). The culture medium was RPMI 1640 or DMEM containing 10% FBS and antibiotics (penicillin 100 U mL^{-1} and streptomycin 100 μg mL^{-1}).

In vitro Cytotoxicity Study. The in vitro cytotoxicity of Len, ZnPc, Len/ZnPc (equimolar mixture), ZnPc-C_0-Len, ZnPc-C_8-Len and ZnPc-C_{12}-Len against MCF7, MCF7/ADR and 4T1 for 72 h was determined by MTT assay. Cells were seeded at 96-well plates (5×10^4 cells per well) with 100 μL DMEM or RPMI 1640 contain 10% FBS. Then the culture medium was removed and 100 μL of drug solution (20 μM for MCF7 and 4T1 cells and 100 μM for

MCF7/ADR cells) or blank culture medium containing 0.5% DMSO (control) was added and incubated for 24 h. After that, drug solution was removed and cells were rinsed twice with PBS and continuously cultured in fresh culture medium. Then cells were exposed to irradiation (660-670 nm, 50 mW cm^{-2}, 10 min) and continuously incubated. The same irradiation was implemented to cells at 48 h and MTT solution was added at 72 h. The absorbance at 570 nm was determined using a microplate reader (ELX800, Bio-Tek, USA). Cell viability was determined by the percentage of the optical density value of the study group over the control group. The in vitro cytotoxicity of Len affect by GSH or BSO was measured by simple pretreatment. Cells were incubated with 2.5 mM GSH or 500 μM BSO for 24 h. Then cells were rinsed twice with PBS and Len in various concentration was added for co-incubation for 24 h. Then cells were rinsed twice with PBS again and fresh culture medium was added for another 48 h. Cell viability was determined by MTT assay. The in vitro cytotoxicity of various concentration of Len, ZnPc and ZnPc-C_8-Len against MCF7, MCF7/ADR and 4T1 cells for 72 h was determined by MTT assay. Drug solution was added and firstly incubated for 24 h. Then drug solution was removed and cells were continuously cultured in fresh culture medium. Cells were exposed to light irradiation (660-670 nm, 50 mW cm^{-2}, 10 min) and then continuously incubated in incubator. The same irradiation was implemented to cells at 48 h and MTT solution was added at 72 h.

Combination index (CI) analysis. The following equation was used to calculate the dose-effect profiles of Len and ZnPc combined in ZnPc-C_8-Len: CI = D/Da + D/Db, where D is the IC_{50} values of ZnPc-C_8-Len. Da and Db represent the IC_{50} values of Len and ZnPc, respectively. CI values less than 1 indicate synergism, CI values equal to 1 indicate an additivity effect, and CI values more than 1 correspond to an antagonism effect.

Glutathione determination. Intracellular GSH was measured as described by instruction of the GSH and GSSG Assay Kit. First, 1×10^6 MCF7 or MCF7/ADR cells were plated in cell culture dish and incubated overnight. Then cells were incubated with 4 μM Len, ZnPc, ZnPc-C_8-Len or 500 μM BSO for 24 h and exposed to irradiation (660-670 nm, 50 mW cm^{-2}, 10 min) after removing drug solution and rinsed with PBS. These cells were treated with trysin and collected by centrifuge, then treated with proper volume of protein removal reagent S. Samples were frozen by liquid nitrogen and thawed at 37 °C for at least three times. After placed at 4 °C for 5 min, the extract was collected by centrifuging at 4 °C at 10000 rpm for 5 min. Proper volume of extract and Proper volume detection solution was mixed in 96-well plates and incubated at 25 °C for 30 min. The intracellular GSH was determined by the absorbance at 405 nm using a microplate reader.

Apoptosis assay. Flow cytometry analysis was used for apoptosis assay. First, MCF7 or MCF7/ADR cells were seeded on 6-well plates (2×10^5 cells per well) and incubated overnight, then the cells were treated with Len, ZnPc and ZnPc-C_8-Len for 24 h. After replacing with the fresh culture medium, cells were exposed to irradiation (50 mW cm^{-2}, 660-670 nm, 10min) at 24 h and 48 h. At 72 h, the cells were digested by trypsin without EDTA, collected in centrifuge tubes, washed with PBS and binding buffer and stained in PI and Annexin-V-FITC containing binding buffer for 15 min, and finally analyzed by Flow Cytometry (Guava EasyCyte 6-2L, Merck Millpore).

Western blot. The change of P-gp, caspase 3 and Bcl-2 was investigated by Western blotting method. Briefly, MCF7/ADR and MCF7 cells were seeded in 6-well plates at a density of 1×10^6 per well. Then the cells were treated with 500 μM BSO, 2.5 mM GSH, 20 μM Len, ZnPc-C_8-Len with or without irradiation. The irradiation (50 mW cm^{-2},660-670 nm) was given at 24 h and

48 h for 10 min once time. Untreated cells were used as the negative control. After 72 h incubation, cells were harvested and the cellular proteins were extracted. The protein concentration was determined using the BCA protein assay. Equal amounts of protein in each treatment were separated by SDS-PAGE and electrotransferred to 0.22 μM PVDF membranes for western blot. And the normalized gray value was analyzed by image analysis software (Image J 1.50i).

Internalization and efflux assay. MCF7 or MCF7/ADR cells were seeded on the sheet glass and incubated overnight. Then the culture medium was replaced with fresh culture medium containing ZnPc-C_8-Len or verapamil was added. The cells of light group was exposed to irradiation (50 mW cm^{-2},660-670 nm) at 6 h and 12 h during 24 h incubation. After that, drug solution was removed and cells were rinsed twice with PBS. The cells were incubated with fresh culture medium for another 24 h. Then the cells were incubated with DCFH-DA for 30 min and exposed to irradiation (50 mW cm^{-2}, 660-670 nm) for 5 min. Finally, the cells were fixed with 4% paraformaldehyde and observed by confocal laser scanning microscope (Olympus FV3000).

Preparation and characterization of PLA_{2000}-PEG_{2000} nanoparticles. The mixed THF solution of ZnPc-C_8-Len and PEG_{2000}-PLA_{2000}, ZnPc and PEG_{2000}-PLA_{2000} or Len and PEG_{2000}-PLA_{2000} (drug: 1 mM, polymer: 8 mM, 100 μL) was slowly added into the distilled water (1 mL) while ultrasound. Then the mixtures were vigorous stirred overnight at room temperature to evaporate the organic solvent. To determine the drug concentration in micelles, micelles were collected by centrifugation and THF was added for demulsification. Then, DMSO was added to dissolve and disperse the ZnPc and ZnPc-C_8-Len. The concentration of Len in micelles was determined by the UV–vis absorbance and the concentration of ZnPc and ZnPc-C_8-Len in micelles was determined by fluorescence assay. The micelles were characterized by Zetasizer

Nano instruments (Zetasizer Nano ZS90) and transmission electron microscopy (JEOL JEM1400).

4.5 In vivo assay

Female BALB/c mice (20 ± 2 g, 5–6 weeks) were obtained from the Laboratory Animal Center of Sun Yat-sen University (Guangzhou, China). All experimental procedures were approved and supervised by the Institutional Animal Care and Use Committee of Sun Yat-sen University. To develop the xenograft tumor model, 4T1 cell suspension was subcutaneously injected into the right flank of each mouse. Tumor volumes were calculated as $(L\times W^2)/2$, (L and W represent the longest and shortest tumor diameter (mm)).

In vivo biodistribution. Mice bearing xenograft tumor were randomly divided into two groups (n=3) and received a tail intravenous injection of free ZnPc-C_8-Len and ZnPc-C_8-Len NPs at a dosage of 2 μmol kg^{-1}. After narcotized, mice were imaged on the detersile area directly via in-vivo imaging Systems (NightOWL LB983, Berthold, Germany). After that, mice were sacrificed and major organs and tumors were excised for imaging. Mean fluorescence intensity (MFI) of excised hearts, livers, spleens, lungs, kidneys and tumor was calculated as fluorescence counts per square millimeter.

In vivo antitumor efficacy. Once the xenograft tumor reached about 100 mm^3, mice were divided randomly into 8 groups (n = 6) and tail intravenous injection with saline, Len NPs, ZnPc NPs, ZnPc-C_8-Len NPs at a dosage of 1 μmol kg^{-1} every four days. And the group with light irradiation was exposed to a laser irradiation (671 nm, 500 mW cm^{-2}, 10 min) at 24 h after drug administration. Tumor volume and body weight were recorded every two days. When the PDT treatment was finished, mice were sacrificed tumors were excised for imaging and recording the

weight. The major organs and tumors were excised for histological examination by standard H&E staining.

4.6 Statistical analysis

Quantitative data were demonstrated by a format as mean ± standard deviation (SD). Anova analysis was used for statistical comparisons. Statistical Package for the Social Sciences version 22 (SPSS 22, SPSS Inc., USA) was used for statistical analyses. $p < 0.05$ was considered as statistically significant, $p < 0.01$ and $p < 0.001$ were considered as highly significant.

Supporting Information

Electronic supplementary information (ESI) available: Chemical synthesis and characterization, Fluorescence Spectroscopy, Photobleaching, Cytotoxicity of GSH and BSO, Cellular drug absorption, TEM images, ROS generation of Len NPs, Intro cytotoxicity of Len NPs.

Conflicts of interest

There are no conficts to declare.

Acknowledgment

We gratefully acknowledge the financial support from National Natural Science Foundation of China (81673369, 81703335), Natural Science Foundation of Guangdong (2017A030313069), Guangdong Medical Research Foundation (A2017114) and the Fundamental Research Funds for the Central Universities (18ykpy25).

Notes and references

1. Hsu, J. L.; Hung, M. C. The role of HER2, EGFR, and other receptor tyrosine kinases in breast cancer. *Cancer Metastasis Rev.* **2016,** *35*, 575-588.
2. Butti, R.; Das, S.; Gunasekaran, V. P.; Yadav, A. S.; Kumar, D.; Kundu, G. C. Receptor tyrosine kinases (RTKs) in breast cancer: signaling, therapeutic implications and challenges. *Mol. Cancer* **2018,** *17*, 34-52.

3. Rosenzweig, S. A. Acquired Resistance to Drugs Targeting Tyrosine Kinases. *Adv. Cancer Res.* **2018,** *138*, 71-98.
4. Backos, D. S.; Franklin, C. C.; Reigan, P. The role of glutathione in brain tumor drug resistance. *Biochem. Pharmacol.* **2012,** *83*, 1005-12.
5. Ballatori, N.; Krance, S. M.; Notenboom, S.; Shi, S.; Tieu, K.; Hammond, C. L. Glutathione dysregulation and the etiology and progression of human diseases. *Biol. Chem.* **2009,** *390*, 191-214.
6. Kawahara, B.; Moller, T.; Hu-Moore, K.; Carrington, S.; Faull, K. F.; Sen, S.; Mascharak, P. K. Attenuation of Antioxidant Capacity in Human Breast Cancer Cells by Carbon Monoxide through Inhibition of Cystathionine beta-Synthase Activity: Implications in Chemotherapeutic Drug Sensitivity. *J. Med. Chem.* **2017,** *60*, 8000-8010.
7. Galluzzi, L.; Senovilla, L.; Vitale, I.; Michels, J.; Martins, I.; Kepp, O.; Castedo, M.; Kroemer, G. Molecular mechanisms of cisplatin resistance. *Oncogene* **2012,** *31*, 1869-83.
8. Pompella, A.; Visvikis, A.; Paolicchi, A.; De Tata, V.; Casini, A. F. The changing faces of glutathione, a cellular protagonist. *Biochem. Pharmacol.* **2003,** *66*, 1499-1503.
9. Balendiran, G. K.; Dabur, R.; Fraser, D. The role of glutathione in cancer. *Cell Biochem. Funct.* **2004,** *22*, 343-352.
10. Estrela, J. M.; Ortega, A.; Obrador, E. Glutathione in cancer biology and therapy. *Crit. Rev. Clin. Lab. Sci.* **2006,** *43*, 143-181.
11. Demeule, M.; Brossard, M.; Turcotte, S.; Regina, A.; Jodoin, J.; Beliveau, R. Diallyl disulfide, a chemopreventive agent in garlic, induces multidrug resistance-associated protein 2 expression. *Biochem. Biophys. Res. Commun.* **2004,** *324*, 937-45.

12. Chen, C.; Wu, C.; Lu, X.; Yan, Z.; Gao, J.; Zhao, H.; Li, S. Coniferyl Ferulate, a Strong Inhibitor of Glutathione S-Transferase Isolated from Radix Angelicae sinensis, Reverses Multidrug Resistance and Downregulates P-Glycoprotein. *Evidence-Based Complementary and Alternative Medicine*. ***2013****, 2013, Article ID 639083.*

13. Spring, B. Q.; Rizvi, I.; Xu, N.; Hasan, T. The role of photodynamic therapy in overcoming cancer drug resistance. *Photochemical & Photobiological Sciences* **2015,** *14*, 1476-1491.

14. Li, H.; Liu, C.; Zeng, Y. P.; Hao, Y. H.; Huang, J. W.; Yang, Z. Y.; Li, R. Nanoceria-Mediated Drug Delivery for Targeted Photodynamic Therapy on Drug-Resistant Breast Cancer. *ACS Appl. Mater. Interfaces* **2016,** *8*, 31510-31523.

15. Zhou, Y.; Huang, F.; Yang, Y.; Wang, P.; Zhang, Z.; Tang, Y.; Shen, Y.; Wang, K. Paraptosis-Inducing Nanomedicine Overcomes Cancer Drug Resistance for a Potent Cancer Therapy. *Small* **2018,** *14*, 1702446.

16. Mao, C.; Zhao, Y.; Li, F.; Li, Z.; Tian, S.; Debinski, W.; Ming, X. P-glycoprotein targeted and near-infrared light-guided depletion of chemoresistant tumors. *J. Control. Release* **2018,** *286*, 289-300.

17. Feng, X.; Jiang, D.; Kang, T.; Yao, J.; Jing, Y.; Jiang, T.; Feng, J.; Zhu, Q.; Song, Q.; Dong, N.; Gao, X.; Chen, J. Tumor-Homing and Penetrating Peptide-Functionalized Photosensitizer-Conjugated PEG-PLA Nanoparticles for Chemo-Photodynamic Combination Therapy of Drug-Resistant Cancer. *ACS Appl. Mater. Interfaces* **2016,** *8*, 17817-17832.

18. Celli, J. P.; Spring, B. Q.; Rizvi, I.; Evans, C. L.; Samkoe, K. S.; Verma, S.; Pogue, B. W.; Hasan, T. Imaging and Photodynamic Therapy: Mechanisms, Monitoring, and Optimization. *Chem. Rev.* **2010,** *110*, 2795-2838.

19. Noh, J.; Kwon, B.; Han, E.; Park, M.; Yang, W.; Cho, W.; Yoo, W.; Khang, G.; Lee, D. Amplification of oxidative stress by a dual stimuli-responsive hybrid drug enhances cancer cell death. *Nat. Commun.* **2015,** *6*, 6907.

20. Zhou, Z.; Song, J.; Nie, L.; Chen, X. Reactive oxygen species generating systems meeting challenges of photodynamic cancer therapy. *Chem. Soc. Rev.* **2016,** *45*, 6597-6626.

21. Wei, X.; Liu, L.; Guo, X.; Wang, Y.; Zhao, J.; Zhou, S. Light-Activated ROS-Responsive Nanoplatform Codelivering Apatinib and Doxorubicin for Enhanced Chemo-Photodynamic Therapy of Multidrug-Resistant Tumors. *ACS Appl. Mater. Interfaces* **2018,** *10*, 17672-17684.

22. Cheung, K. K. Y.; Chan, J. Y. W.; Fung, K. P. Antiproliferative effect of pheophorbide a-mediated photodynamic therapy and its synergistic effect with doxorubicin on multiple drug-resistant uterine sarcoma cell MES-SA/Dx5. *Drug Chem. Toxicol.* **2013,** *36*, 474-483.

23. Wang, L. M.; Sun, Q.; Wang, X.; Wen, T.; Yin, J. J.; Wang, P. Y.; Bai, R.; Zhang, X. Q.; Zhang, L. H.; Lu, A. H.; et al. Using Hollow Carbon Nanospheres as a Light-Induced Free Radical Generator to Overcome Chemotherapy Resistance. *J. Am. Chem. Soc.* **2015,** *137*, 1947-1955.

24. Matsui, J.; Funahashi, Y.; Uenaka, T.; Watanabe, T.; Tsuruoka, A.; Asada, M. Multi-kinase inhibitor E7080 suppresses lymph node and lung metastases of human mammary breast tumor MDA-MB-231 via inhibition of vascular endothelial growth factor-receptor (VEGF-R) 2 and VEGF-R3 kinase. *Clin. Cancer Res.* **2008,** *14*, 5459-65.

25. Shumaker, R. C.; Aluri, J.; Fan, J.; Martinez, G.; Thompson, G. A.; Ren, M. Effect of rifampicin on the pharmacokinetics of Len in healthy adults. *Clin. Drug Investig.* **2014,** *34*, 651-659.

26. Zhang, F. L.; Song, M. R.; Yuan, G. K.; Ye, H. N.; Tian, Y.; Huang, M. D.; Xue, J. P.; Zhang, Z. H.; Liu, J. Y. A Molecular Combination of Zinc(II) Phthalocyanine and Tamoxifen Derivative for Dual Targeting Photodynamic Therapy and Hormone Therapy. *J. Med. Chem.* **2017,** *60*, 6693-6703.

27. Huang, Z.; Huang, L.; Huang, Y.; He, Y.; Sun, X.; Fu, X.; Xu, X.; Wei, G.; Chen, D.; Zhao, C. Phthalocyanine-based coordination polymer nanoparticles for enhanced photodynamic therapy. *Nanoscale* **2017,** *9*, 15883-15894.

28. Lopes-Rodrigues, V.; Di Luca, A.; Mleczko, J.; Meleady, P.; Henry, M.; Pesic, M.; Cabrera, D.; van Liempd, S.; Lima, R. T.; O'Connor, R.; et al. Identification of the metabolic alterations associated with the multidrug resistant phenotype in cancer and their intercellular transfer mediated by extracellular vesicles. *Sci. Rep.* **2017,** *7*, 44541.

29. Chatterjee, A. Reduced Glutathione: A Radioprotector or a Modulator of DNA-Repair Activity? *Nutrients* **2013,** *5*, 525-542.

30. Cho, S. G.; Lee, Y. H.; Park, H. S.; Ryoo, K.; Kang, K. W.; Park, J.; Eom, S. J.; Kim, M. J.; Chang, T. S.; Choi, S. Y.; et al. Glutathione S-transferase mu modulates the stress-activated signals by suppressing apoptosis signal-regulating kinase 1. *J. Biol. Chem.* **2001,** *276*, 12749-12755.

31. Colvin, O. M.; Friedman, H. S.; Gamcsik, M. P.; Fenselau, C.; Hilton, J. Role of glutathione in cellular resistance to alkylating agents. *Adv. Enzyme Regul.* **1993,** *33*, 19-26.

32. Rudin, C. M.; Yang, Z.; Schumaker, L. M.; VanderWeele, D. J.; Newkirk, K.; Egorin, M. J.; Zuhowski, E. G.; Cullen, K. J. Inhibition of glutathione synthesis reverses Bcl-2-mediated cisplatin resistance. *Cancer Res.* **2003,** *63*, 312-318.

33. Hardwick, J. M.; Soane, L. Multiple Functions of BCL-2 Family Proteins. *Cold Spring Harb. Perspect. Biol.* **2013,** *5*, a008722.

34. McIlwain, D. R.; Berger, T.; Mak, T. W. Caspase functions in cell death and disease. *Cold Spring Harb. Perspect. Biol.* **2013,** *5*, a008656.

35. Koziolova, E.; Chytil, P.; Etrych, T.; Janouskova, O. Ability of polymer-bound P-glycoprotein inhibitor ritonavir to overcome multidrug resistance in various resistant neuroblastoma cell lines. *Anticancer Drugs* **2017,** *28*, 1126-1130.

36. Chou, T.C. Chemotherapy: synergism and antagonism. In *Encyclopedia of Cancer (Second Edition)*. Bertino, J. R. Academic Press: New York, 2002; pp 473-484.

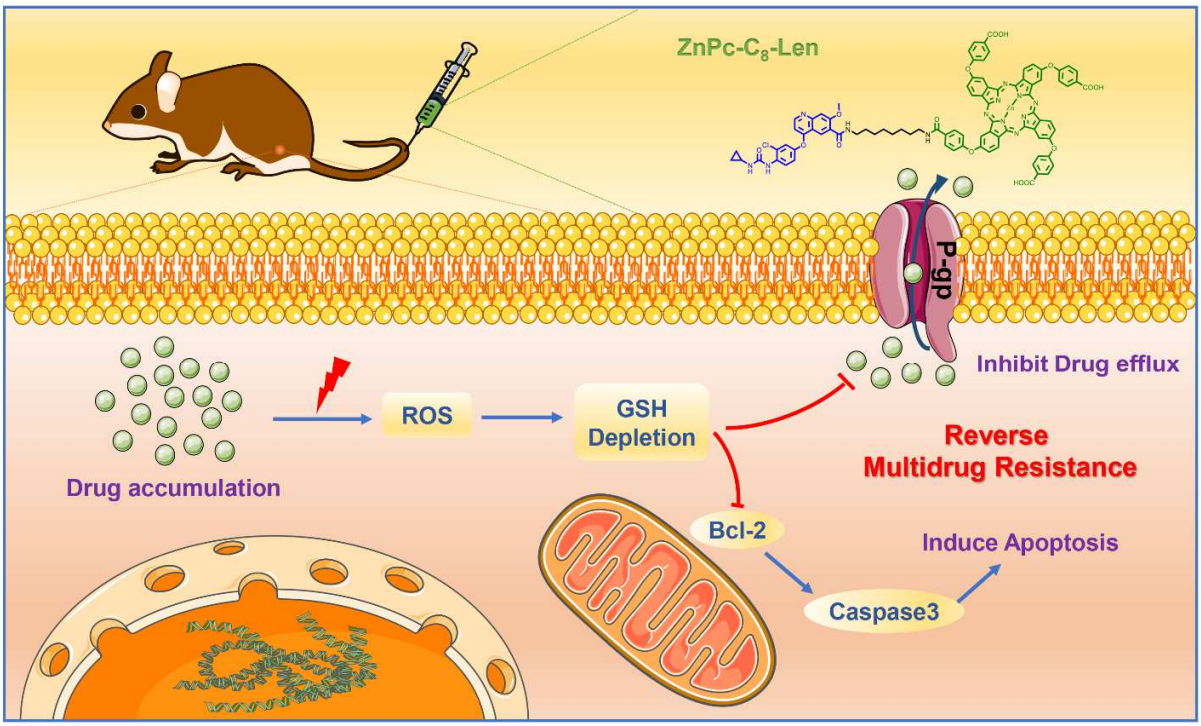

Scheme 1. Schematic illustration of mechanism for drug resistance reversal by ZnPc-C_8-Len.

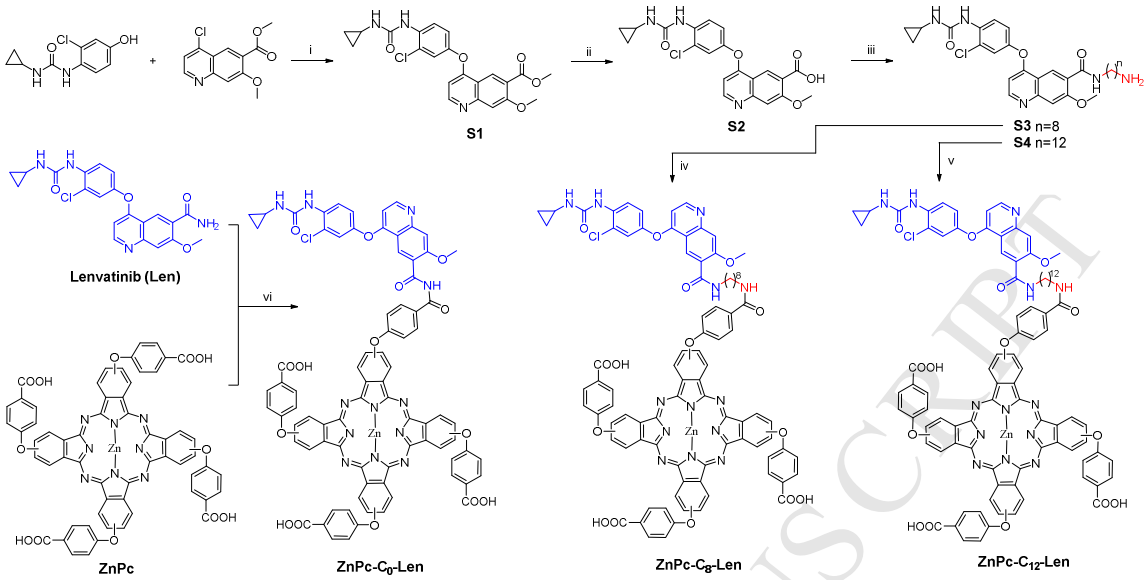

Scheme 2. Synthesis of conjugate ZnPc-C_n-Len. Reagents and conditions: (i) K_2CO_3, DMF, 75□, 30 min, and then rt, 2 h. (ii) NaOH, MeOH, THF, 70□, 2.5 h. (iii) EDCI, BtOH, DMF, rt, 2 h, and then 1,8-Diaminooctane or 1,12-Dodecanediamine, rt, 24 h. (iv-vi) ZnPc, EDCI, HoBt, DIPEA, DMF, rt, 24 h.

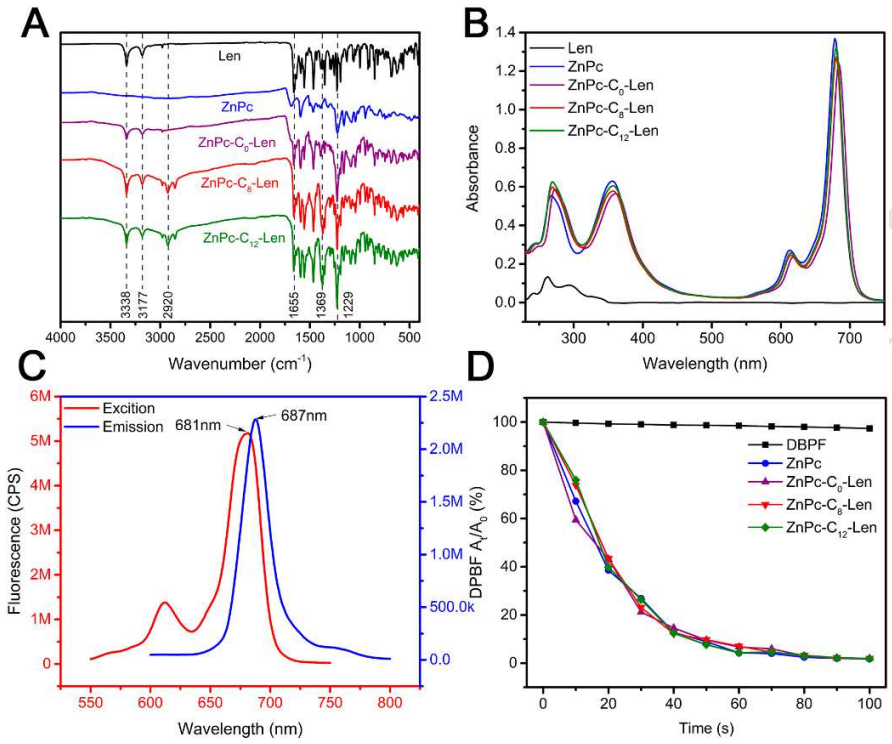

Figure 1. Spectroscopy and photosensitization ability of ZnPc-C_n-Len. The FTIR spectrum (A) and the UV/vis absorbance (B) of Len, ZnPc, ZnPc-C_0-Len, ZnPc-C_8-Len and ZnPc-C_{12}-Len. (C) Excitation and Emission fluorescence spectroscopy of ZnPc-C_8-Len in DMSO. (D) The ROS generation of ZnPc, ZnPc-C_0-Len, ZnPc-C_8-Len and ZnPc-C_{12}-Len in DMSO.

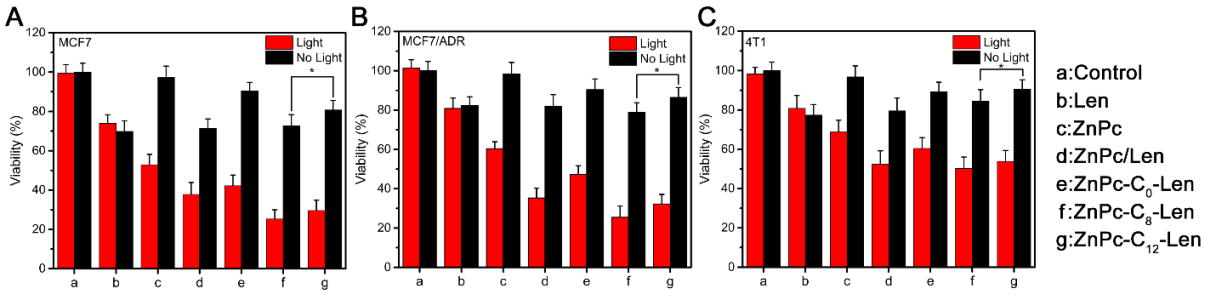

Figure 2. *In vitro* cytotoxicity of Len, ZnPc, ZnPc/Len (equimolar mixture), ZnPc-C_0-Len, ZnPc-C_8-Len and ZnPc-C_{12}-Len against MCF7 cells (A), MCF7/ADR cells (B) and 4T1 cells (C) (20 μM for MCF7 and 4T1 cells and 100 μM for MCF7/ADR cells) for 72 h in the present or absence of irradiation (660-670 nm, 50 mW cm^{-2}, 10 min). Data are expressed as mean ± standard deviation (SD). (n=6, *$p < 0.05$)

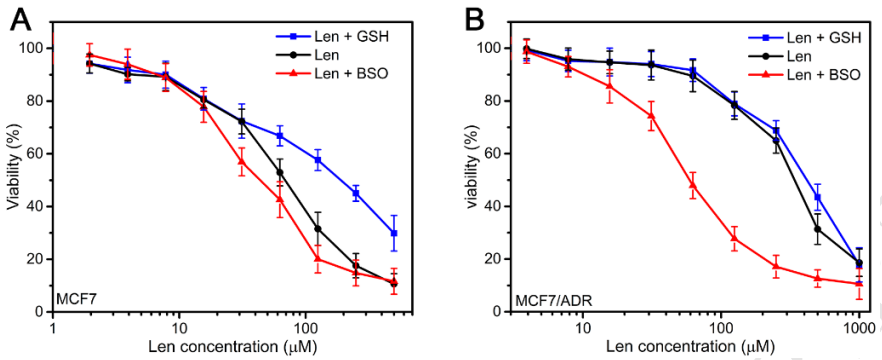

Figure 3. Comparison of the in vitro cytotoxicity of Len with the pretreatment of GSH (2.5 mM) or BSO (500 μM) against MCF7 (A) or MCF7/ADR (B) cells. Data are expressed as mean ± standard deviation (SD). (n=6).

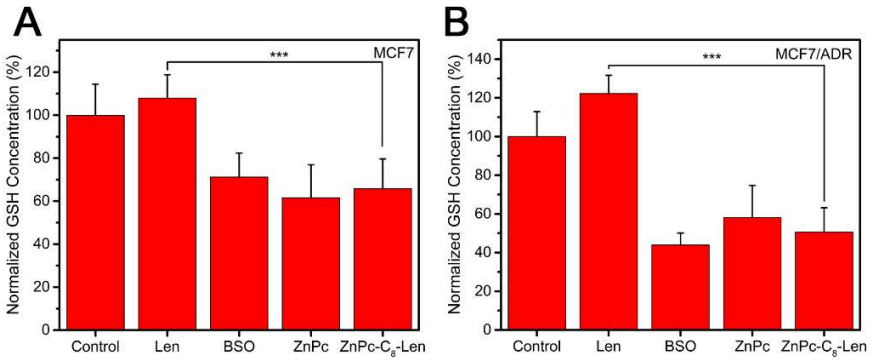

Figure 4. Investigation of intracellular GSH level change with the incubation of Len (4 μM), BSO (500 μM), ZnPc (4 μM) and ZnPc-C_8-Len (4 μM) against MCF7 (A) and MCF7/ADR (B) cells under irradiation (660-670 nm, 50 mW cm^{-2}, 10 min). Data are expressed as mean ± standard deviation (SD). (n=3, ***$p < 0.001$)

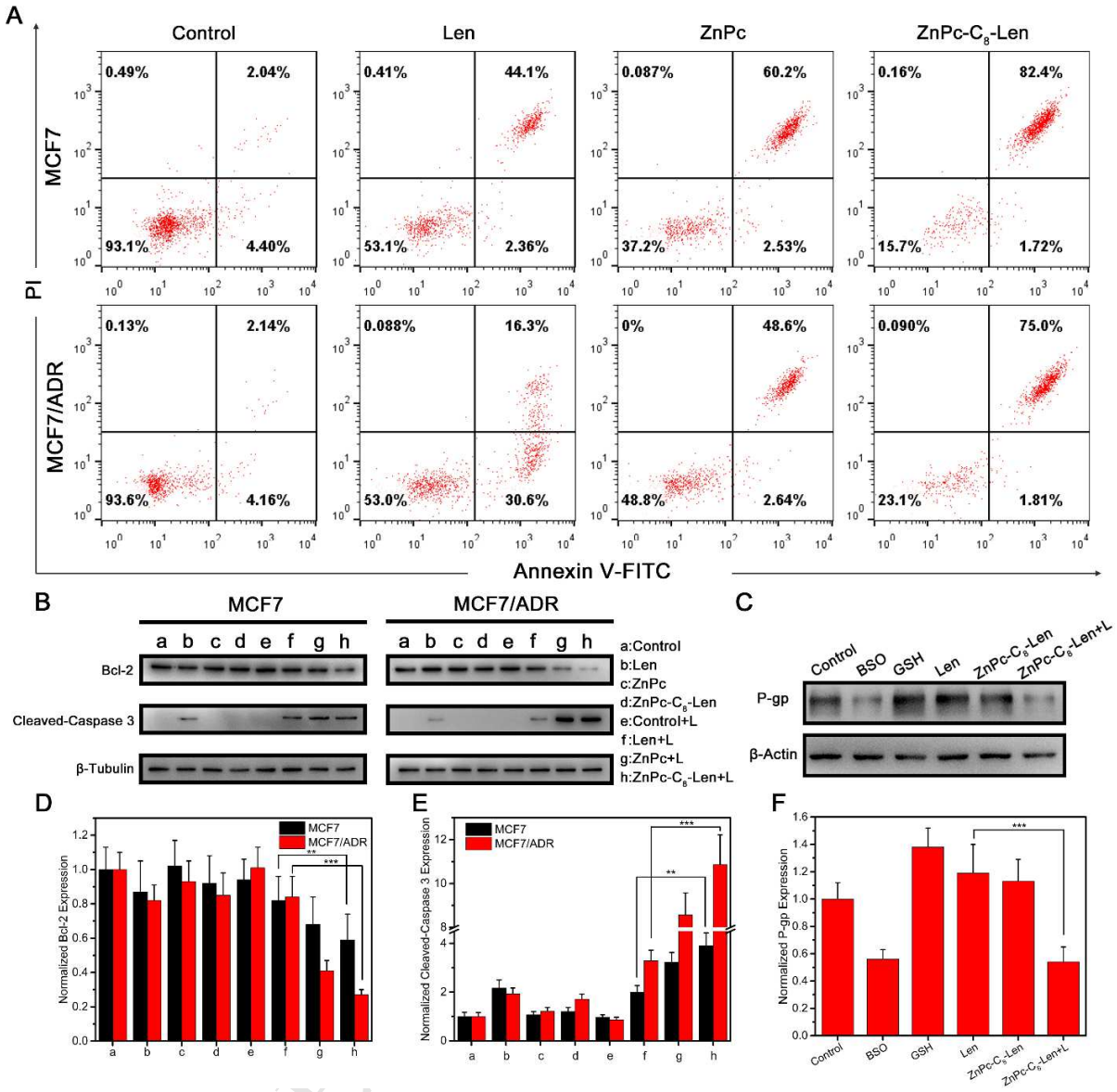

Figure 5. Mechanism of MDR Reversal. (A) Cellular apoptosis assay of Len, ZnPc and ZnPc-C_8-Len against MCF7 and MCF7/ADR cells (20 μM for MCF7 cells and 100 μM for MCF7/ADR cells) in the presence of irradiation (660-670 nm, 50 mW cm-2, 10 min). (B) Regulation of apoptosis-related Bcl-2 and cleaved-caspase 3 protein expressions in MCF7 and MCF7/ADR cells after treatment were detected with western blot analysis. β-tubulin was used as an internal control. (C) Regulation of MDR-related P-gp protein expression in MCF7/ADR cells after treatment. β-actin was used as an internal control. Quantification of protein expression levels based on western blotting results of Bcl-2 (D), cleaved-caspase 3 (E) and P-gp (F). Data are expressed as mean ± standard deviation (SD). (n=3, **$p < 0.01$, ***$p < 0.001$)

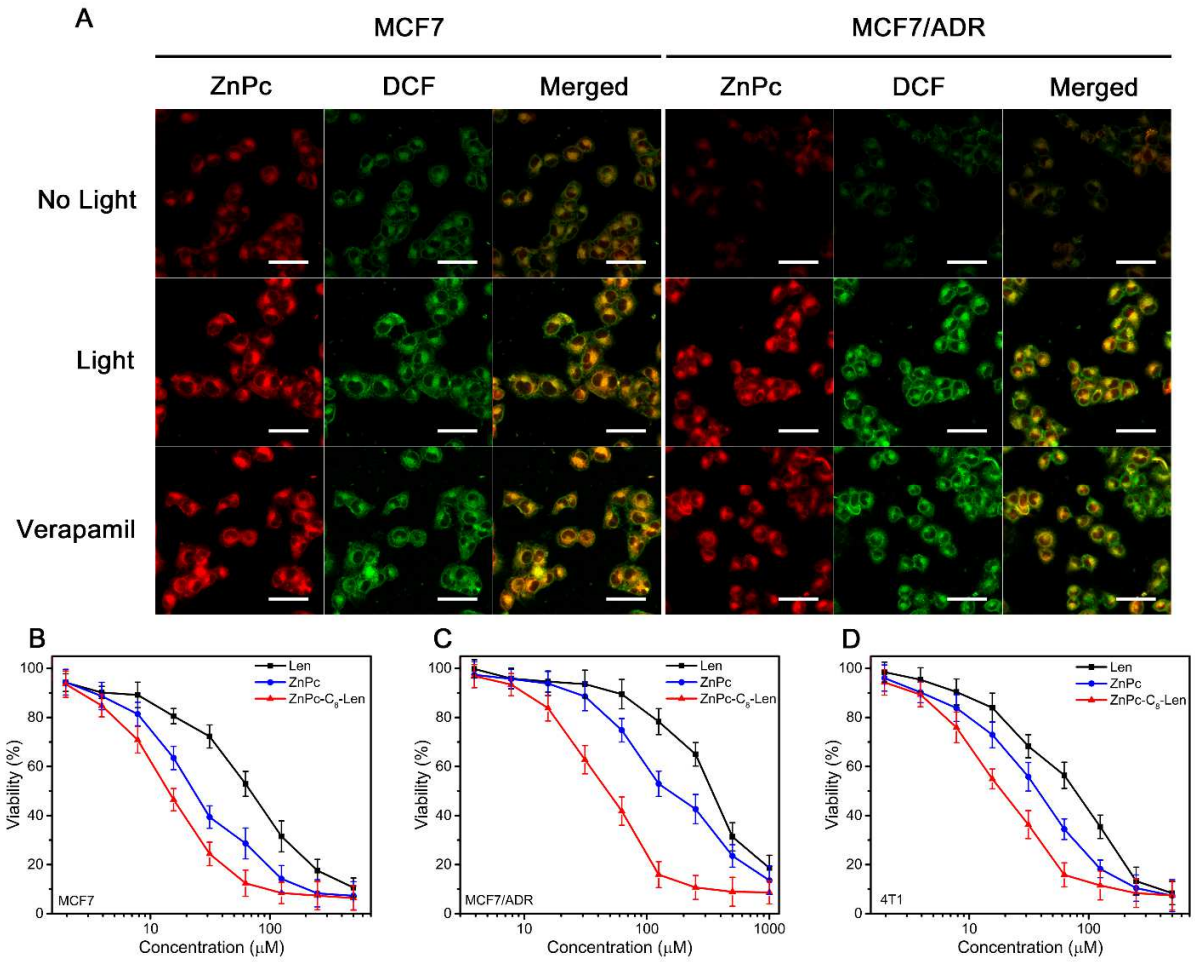

Figure 6. Cellular drug efflux assay and in vitro cytotoxicity assay of ZnPc-C_8-Len under the irradiation (660-670 nm, 50 mW cm^{-2}, 10 min). (A) Cellular drug efflux was determined by CLSM in MCF7 and MCF7/ADR cells. ZnPc channel represented intracellular ZnPc-C_8-Len and showed in red color. DCF channel represented intracellular ROS and showed in green color. (scale bar = 50 μm). The vitro viability of Len, ZnPc and ZnPc-C_8-Len against MCF7 (B), MCF7/ADR (C) and 4T1 (D) cells in different concentration exposing to irradiation. Data are expressed as mean ± standard deviation (SD). (n=6)

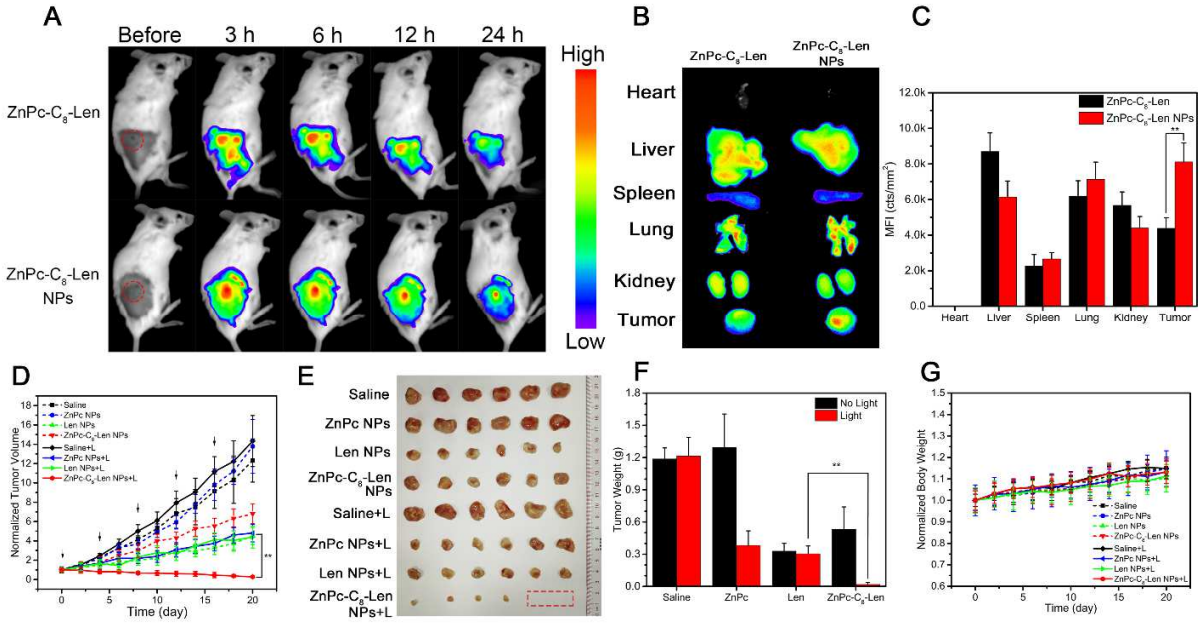

Figure 7. *In vivo* biodistribution studies and anti-tumor evaluation on balb/c mice bearing 4T1 xenografts. (A) Time-lapsed in vivo fluorescence imaging after single intravenous injection at a dosage of 2 μmol kg^{-1} (Tumors were labeled in red dash circles) (B) Ex vivo fluorescence images of excised major organs and tumors at 24 h post-injection (C) Semi-quantitative analysis of fluorescence signals of major organs and tumors at 24 h post-injection. (n=3, **p < 0.01) (D) The relative tumor volume (V/V_0) during the treatment of Saline, ZnPc NPs, Len NPs and ZnPc-C_8-Len NPs with or without irradiation (671 nm, 500 mW cm^{-2}, 10 min). (Arrows for treatment times, each injection at a dosage of 1 μmol kg^{-1}) Photograph (E) and weight (F) of the tumors after PDT treatment. (G) The relative body weight of mice during the PDT treatment. Data are expressed as mean ± standard deviation (SD). (solid line for irradiation, dash line for no irradiation, n=6, **p < 0.01)

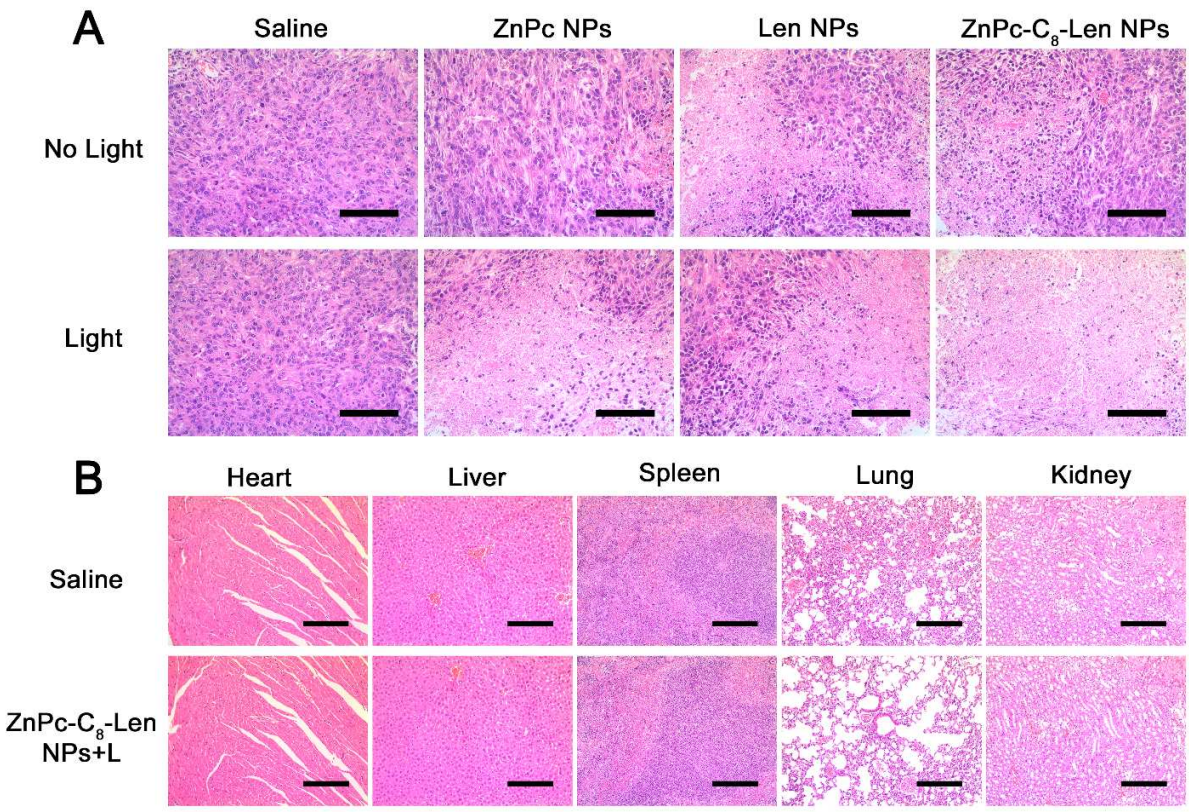

Figure 8. H&E images of the tumor section (A) and major organs section (B) after different treatments showing cytoplasm (red) and cell nucleus (blue) (Scale bar = 50 mm).

Graphical abstracts